

# FFT-accelerated computation of the Dirichlet-to-Neumann map for inhomogeneous exterior Helmholtz problems using the method of fundamental solutions

Takemi Shigeta<sup>1,\*</sup>

*Laboratory of Applied Mathematics, Showa Pharmaceutical University  
3-2-1 Higashi-Tamagawagakuen, Machida, Tokyo 194-8543, Japan*

---

## Abstract

An efficient numerical method is proposed for computing the Dirichlet-to-Neumann (DtN) map associated with the exterior Dirichlet problem for the two-dimensional Helmholtz equation with an inhomogeneous term. The exterior solution is approximated by the method of fundamental solutions (MFS). When the source and collocation points are equally spaced on concentric circles, the coefficient matrices arising in the discretization become circulant, which enables efficient evaluation of the discrete DtN map by the fast Fourier transform (FFT). By incorporating the boundary condition defined by the DtN map into a finite element formulation, the original exterior problem posed on an unbounded domain is reduced to an equivalent problem on a bounded computational domain, which can then be solved by the finite element method (FEM). Numerical examples show that the proposed MFS-based approach computes the DtN map with high accuracy, and that the FEM incorporating the boundary condition defined by the DtN map yields accurate solutions for exterior Helmholtz problems with an inhomogeneous term posed on unbounded domains.

*Keywords:* Circulant matrix, Dirichlet-to-Neumann map, Domain decomposition method, Exterior boundary value problem, Fast Fourier transform, Inhomogeneous Helmholtz equation, Method of fundamental solutions, Transparent boundary condition

---

## 1. Introduction

Exterior boundary value problems for elliptic partial differential equations arise in many applications, including wave propagation and scattering. A typical example is the exterior inhomogeneous Helmholtz problem, which appears in

---

\*Corresponding author

<sup>1</sup>Professor

time-harmonic acoustic radiation when a localized source is situated near an obstacle. For instance, waves emitted by a vibrating device or a loudspeaker in the vicinity of a rigid body can be modeled by the Helmholtz equation with a compactly supported source term in the exterior domain. Since the radiated field propagates into an unbounded domain, an accurate treatment of the radiation condition is essential.

Among numerical methods for partial differential equations, the finite element method (FEM) is one of the most reliable and widely used methods. However, the FEM is essentially designed for problems posed on bounded computational domains and cannot directly handle exterior problems on unbounded domains. Therefore, in order to solve exterior Helmholtz problems by the FEM, it is necessary to replace the original problem by an equivalent problem posed on a bounded domain.

In this context, the Dirichlet-to-Neumann (DtN) map plays a central role. The DtN map associates Dirichlet data prescribed on a boundary with the corresponding normal derivative. Once the DtN map is available on such a boundary, the original exterior problem can be reformulated as a boundary value problem on a bounded computational domain equipped with a transparent boundary condition (TBC) [2, 14]. This makes it possible to solve the original problem on an unbounded domain by using the FEM on a bounded computational domain.

A classical approach to exterior boundary value problems is the Dirichlet–Neumann alternating method (D–N method) [5, 9, 15, 19]. This is an iterative domain decomposition method [12], in which an artificial boundary divides the domain into two subdomains: the inhomogeneous equation is solved in the interior subdomain, while the homogeneous equation is solved in the exterior subdomain. Its convergence rate depends strongly on the relaxation parameter used to update the boundary values on the artificial boundary.

For the two-dimensional Poisson equation, when both the boundary of the original problem and the artificial boundary are concentric circles, the optimal constant relaxation parameter yielding the fastest convergence is known [18]. The author further derived an optimal variable relaxation parameter, in which the relaxation parameter is chosen optimally at each iteration [15]. Although the assumption of circular boundaries simplifies the theoretical analysis, the boundary of the original problem is not necessarily circular in general. For this reason, it is meaningful to consider artificial boundaries of more general shapes [14]. Another possible approach is to use the conformal mapping to reduce the problem to one with a circular boundary [11], so that the optimal variable relaxation parameter can be applied.

However, although the conformal mapping is effective for the two-dimensional Poisson equation, its application to the Helmholtz equation becomes difficult because the wavenumber is transformed into a spatially varying coefficient. Moreover, the conformal mapping is not available in three dimensions. These difficulties motivate the development of a direct numerical method that does not rely on iterative relaxation schemes restricted to circular boundaries or on the conformal mapping.

In this paper, we develop such a direct numerical method for the exterior

Dirichlet problem of the two-dimensional inhomogeneous Helmholtz equation. By introducing a circular artificial boundary, we represent the effect of the unbounded subdomain outside the artificial boundary through the DtN map and impose the resulting condition as a TBC on the artificial boundary [2, 14]. This reduces the original exterior problem to a bounded domain problem, which can then be solved by the FEM.

To construct the DtN map numerically, we employ the method of fundamental solutions (MFS) [1, 3, 6, 7, 8, 13], a boundary-type meshfree method for partial differential equations. In the MFS, the solution is approximated by a finite linear combination of fundamental solutions with source points placed outside the computational domain, and the expansion coefficients are determined by enforcing the boundary conditions at collocation points on the boundary. Since the MFS does not require mesh generation or volume integration, it is simple to implement, and it is well known to yield highly accurate approximations for problems with smooth geometries and smooth solutions. Furthermore, by exploiting the circulant structure of the resulting matrices, the computation of the discrete DtN map can be carried out efficiently by the fast Fourier transform (FFT) [4, 10, 11, 17].

In a previous paper by the author, a related FFT-based numerical computation of the DtN map for the homogeneous exterior Helmholtz problem was presented in [16]. In the present paper, we extend this line of research to the inhomogeneous Helmholtz equation. The main points are twofold: first, the DtN map on an artificial boundary is computed accurately and efficiently by the MFS together with the FFT; second, the resulting DtN-based TBC is incorporated into a finite element formulation, which enables inhomogeneous exterior Helmholtz problems on unbounded domains to be solved on a bounded computational domain.

The remainder of this paper is organized as follows. Section 2 formulates the exterior boundary value problem for the two-dimensional inhomogeneous Helmholtz equation and introduces a circular artificial boundary together with the DtN map. Section 3 presents the MFS formulation for the exterior problem together with the resulting discretization of the DtN map. Section 4 develops an FFT-based algorithm for the efficient computation of the discrete DtN map by exploiting the circulant structure of the matrices. Section 5 describes the finite element discretization with the DtN-based TBC. Section 6 presents numerical examples demonstrating the high accuracy of the MFS-based DtN map, the efficiency of the FFT-based computation, and the successful solution of inhomogeneous exterior problems in unbounded domains by the FEM combined with the DtN-based TBC. Finally, Section 7 concludes the paper.

## 2. Problem formulation

Throughout this paper, we identify  $\mathbb{R}^2$  with  $\mathbb{C}$  via  $(x, y) \mapsto x + iy$ , and write  $z = x + iy$ , where  $i := \sqrt{-1}$  denotes the imaginary unit. Let  $R \in C[0, 2\pi)$  be a

given function. We consider the simple closed curve

$$\Gamma := \{R(\theta)e^{i\theta} : 0 \leq \theta < 2\pi\}$$

and the simply connected bounded domain  $\Omega_0 \subset \mathbb{C}$  enclosed by  $\Gamma$ . Without loss of generality we assume that  $0 \in \Omega_0$ . We consider the following exterior Dirichlet problem for the inhomogeneous Helmholtz equation, in which the unknown function  $u \in H_{\text{loc}}^1(\mathbb{C} \setminus \overline{\Omega_0})$  is to be determined:

$$-(\Delta u + \kappa^2 u) = f \quad \text{in } \mathbb{C} \setminus \overline{\Omega_0}, \quad (2.1a)$$

$$u = g \quad \text{on } \Gamma, \quad (2.1b)$$

$$\frac{\partial u}{\partial r} - i\kappa u = o(r^{-1/2}) \quad \text{as } r := |z| \rightarrow \infty, \quad (2.1c)$$

where  $\Delta := \partial^2/\partial x^2 + \partial^2/\partial y^2$  denotes the Laplace operator,  $\kappa > 0$  a given wavenumber,  $f \in L^2(\mathbb{C} \setminus \overline{\Omega_0})$  a given inhomogeneous term, and  $g \in H^{1/2}(\Gamma)$  the prescribed Dirichlet data. Equation (2.1c) is the Sommerfeld radiation condition, which ensures that the wave propagates outward toward infinity. The support of  $f$ , defined by

$$\text{supp } f := \overline{\{z \in \mathbb{C} \setminus \overline{\Omega_0} : f(z) \neq 0\}},$$

is assumed to be bounded.

We introduce a circular artificial boundary  $\Gamma_0 := \{R_0 e^{i\theta} : 0 \leq \theta < 2\pi\}$  ( $R_0 > R(\theta)$ ) so that the support of  $f$  is enclosed by  $\Gamma_0$ , and decompose the unbounded domain  $\mathbb{C} \setminus \overline{\Omega_0}$  into the bounded subdomain  $\Omega$  ( $\supset \text{supp } f$ ) and the remaining unbounded subdomain  $\Omega_e$ . Note that  $f = 0$  in  $\Omega_e$ . Let  $v$  denote the restriction of the unknown function  $u$  to  $\Omega_e$ . For simplicity, we continue to denote the restriction of  $u$  to  $\Omega$  by  $u$ . Then the following coupling conditions hold on the artificial boundary  $\Gamma_0$ :

$$u = v, \quad \frac{\partial u}{\partial n} = \frac{\partial v}{\partial n} \quad \text{on } \Gamma_0, \quad (2.2)$$

where  $n = n(z) := z/R_0$  denotes the outward unit normal vector on  $\Gamma_0$  with respect to the domain  $\Omega$  (see Fig. 1).

The Dirichlet-to-Neumann (DtN) map  $\Lambda : H^{1/2}(\Gamma_0) \rightarrow H^{-1/2}(\Gamma_0)$  is defined by

$$\Lambda \lambda := \frac{\partial v}{\partial n}, \quad \forall \lambda \in H^{1/2}(\Gamma_0), \quad (2.3)$$

where  $v \in H_{\text{loc}}^1(\Omega_e)$  denotes the solution of the following exterior Dirichlet problem for the Helmholtz equation:

$$\Delta v + \kappa^2 v = 0 \quad \text{in } \Omega_e, \quad (2.4a)$$

$$v = \lambda \quad \text{on } \Gamma_0, \quad (2.4b)$$

$$\frac{\partial v}{\partial r} - i\kappa v = o(r^{-1/2}) \quad \text{as } r \rightarrow \infty. \quad (2.4c)$$

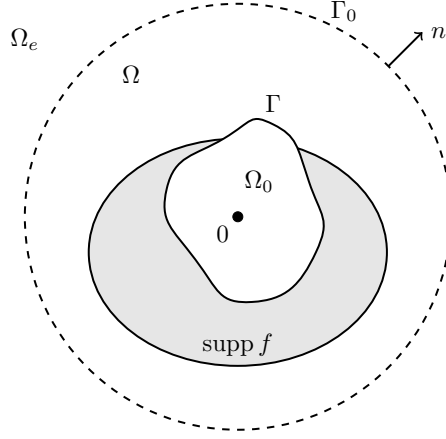


Figure 1: Domain decomposition by introducing an artificial boundary

Then, from the coupling condition (2.2) and the DtN map (2.3), the original problem (2.1) can be reformulated equivalently as the following mixed boundary value problem posed on the doubly connected bounded domain, in which the unknown function  $u \in H^1(\Omega)$  is to be determined:

$$-(\Delta u + \kappa^2 u) = f \quad \text{in } \Omega, \quad (2.5a)$$

$$u = g \quad \text{on } \Gamma, \quad (2.5b)$$

$$\frac{\partial u}{\partial n} - \Lambda u = 0 \quad \text{on } \Gamma_0. \quad (2.5c)$$

Equation (2.5c) is called the transparent boundary condition (TBC), which allows outgoing waves to pass through the artificial boundary without generating spurious reflections, so that the solution inside the computational domain agrees with the solution of the original exterior problem [2].

### 3. Method of fundamental solutions

#### 3.1. Discretization of the solution

For  $\zeta \in \mathbb{C}$ , the fundamental solution  $\Phi_\kappa(\cdot, \zeta)$  to the Helmholtz operator  $-(\Delta + \kappa^2)$  is defined by

$$-(\Delta + \kappa^2)\Phi_\kappa(z, \zeta) = \delta(z - \zeta)$$

in the sense of distributions, and is given by

$$\Phi_\kappa(z, \zeta) := \frac{i}{4} H_0^{(1)}(\kappa|z - \zeta|), \quad z, \zeta \in \mathbb{C}, \quad z \neq \zeta,$$

where  $\delta(z - \zeta)$  denotes the Dirac delta distribution concentrated at the point  $\zeta$ , and  $H_\nu^{(1)}$  the Hankel function of the first kind of order  $\nu$ .

We choose  $N$  distinct source points  $\{\zeta_j\}_{j=0}^{N-1} \subset \mathbb{C} \setminus \overline{\Omega_e}$  equally spaced on a fictitious circle centered at the origin with radius  $\rho$  ( $0 < \rho < R_0$ ) by setting

$$\omega := e^{2\pi i/N}, \quad \zeta_j := \rho\omega^j, \quad j = 0, 1, \dots, N-1,$$

where  $\omega$  is the primitive  $N$ th root of unity. Here and throughout the paper, Roman letters are used for the physical boundary and its points, while Greek letters are reserved for the fictitious circle and source points. Then the solution of the exterior Dirichlet problem (2.4) is discretized by the method of fundamental solutions (MFS) [1, 3, 6, 7, 8, 13] as

$$v(z) \approx v^{(N)}(z) := \sum_{j=0}^{N-1} \alpha_j \Phi_\kappa(z, \zeta_j), \quad z \in \overline{\Omega_e} := \Omega_e \cup \Gamma_0, \quad (3.1)$$

where  $\{\alpha_j\}_{j=0}^{N-1} \subset \mathbb{C}$  are unknown expansion coefficients to be determined later.

Since the functions  $\{\Phi_\kappa(\cdot, \zeta_j)\}_{j=0}^{N-1}$ , which are used as MFS basis functions, satisfy the Helmholtz equation (2.4a) and the Sommerfeld radiation condition (2.4c), the approximate solution (3.1) also satisfies (2.4a) and (2.4c). Therefore, it remains only to impose the boundary condition (2.4b).

Next, we choose  $N$  distinct collocation points  $\{z_k\}_{k=0}^{N-1} \subset \Gamma_0$  equally spaced along the circular boundary  $\Gamma_0$ , defined by

$$z_k := R\omega^k, \quad k = 0, 1, \dots, N-1.$$

Substituting  $z = z_k$  into the Dirichlet condition (2.4b), we obtain the following linear system of equations for  $\{\alpha_j\}_{j=0}^{N-1} \subset \mathbb{C}$ :

$$v^{(N)}(z_k) = \sum_{j=0}^{N-1} \alpha_j \Phi_\kappa(z_k, \zeta_j) = \lambda(\theta_k), \quad k = 0, 1, \dots, N-1,$$

or, in matrix-vector form,

$$C_0 \boldsymbol{\alpha} = \boldsymbol{\lambda}, \quad (3.2)$$

where the matrix  $C_0 \in \mathbb{C}^{N \times N}$  and the vectors  $\boldsymbol{\alpha}, \boldsymbol{\lambda} \in \mathbb{C}^N$  are defined by

$$(C_0)_{k,j} := \Phi_\kappa(z_k, \zeta_j), \quad (\boldsymbol{\alpha})_j := \alpha_j, \quad (\boldsymbol{\lambda})_k := \lambda(\theta_k), \quad k, j = 0, 1, \dots, N-1.$$

If  $C_0$  is nonsingular, then the unknown expansion coefficients are uniquely determined as

$$\boldsymbol{\alpha} = C_0^{-1} \boldsymbol{\lambda}. \quad (3.3)$$

Substituting (3.3) into (3.1), we obtain an approximate solution to (2.4) in the whole computational domain  $\overline{\Omega_e}$ .

### 3.2. Discretization of the DtN map

Taking the normal derivative of (3.1) and substituting  $z = z_k$ , we obtain the approximation of the normal derivative of  $v$  at the collocation points on  $\Gamma_0$  as follows:

$$\frac{\partial v^{(N)}}{\partial n}(z_k) = \sum_{j=0}^{N-1} \alpha_j \frac{\partial \Phi_\kappa}{\partial n}(z_k, \zeta_j), \quad k = 0, 1, \dots, N-1,$$

or, in matrix-vector form,

$$\boldsymbol{\mu} = C_1 \boldsymbol{\alpha}, \quad (3.4)$$

where the vector  $\boldsymbol{\mu} \in \mathbb{C}^N$  and the matrix  $C_1 \in \mathbb{C}^{N \times N}$  are defined by

$$(\boldsymbol{\mu})_k := \frac{\partial v^{(N)}}{\partial n}(z_k), \quad (C_1)_{k,j} := \frac{\partial \Phi_\kappa}{\partial n}(z_k, \zeta_j), \quad k, j = 0, 1, \dots, N-1.$$

The matrices  $C_l$  ( $l = 0, 1$ ) can be interpreted as matrices whose entries are given by the  $l$ -th derivatives of the fundamental solution. The normal derivative of the function  $\Phi_\kappa(\cdot, \zeta_j)$  is explicitly expressed as

$$\frac{\partial \Phi_\kappa}{\partial n}(z, \zeta_j) = -\frac{i\kappa}{4} H_1^{(1)}(\kappa|z - \zeta_j|) \frac{(z - \zeta_j) \cdot \mathbf{n}(z)}{|z - \zeta_j|},$$

where we define the Euclidean inner product of  $z_1 = x_1 + iy_1$  and  $z_2 = x_2 + iy_2$  by

$$z_1 \cdot z_2 := \operatorname{Re}(z_1 \overline{z_2}) = x_1 x_2 + y_1 y_2.$$

Substituting (3.3) into (3.4), we obtain

$$C_1 C_0^{-1} \boldsymbol{\lambda} = \boldsymbol{\mu}. \quad (3.5)$$

Equation (3.5) corresponds to a discretization of (2.3). Therefore, the matrix

$$\Lambda^{(N)} := C_1 C_0^{-1} \quad (3.6)$$

can be regarded as a discrete approximation of the DtN map  $\Lambda$ .

## 4. Efficient computation using the FFT

In this section we describe an efficient method for computing the discrete DtN map. The key observation is that the matrices arising from the MFS discretization become circulant when both the source points and collocation points are equally spaced on circles. This structure enables the discrete DtN map to be computed efficiently by the FFT [4, 10, 11, 17].

#### 4.1. Discrete Fourier Transform

Let  $\mathbf{c} = (c_0, c_1, \dots, c_{N-1})^T \in \mathbb{C}^N$ . The discrete Fourier transform (DFT) of  $\mathbf{c}$  is defined by

$$\widehat{c}_k := \sum_{j=0}^{N-1} c_j \omega^{jk}, \quad k = 0, 1, \dots, N-1, \quad (4.1)$$

where  $\omega = e^{2\pi i/N}$  as defined above.

The DFT (4.1) can be written in the matrix form:

$$\widehat{\mathbf{c}} = \mathcal{F}(\mathbf{c}) := W\mathbf{c}$$

with  $\widehat{\mathbf{c}} = (\widehat{c}_0, \widehat{c}_1, \dots, \widehat{c}_{N-1})^T \in \mathbb{C}^N$ , where  $W \in \mathbb{C}^{N \times N}$  is the DFT matrix defined by

$$(W)_{k,j} := \omega^{jk}, \quad k, j = 0, 1, \dots, N-1.$$

Then  $W$  satisfies

$$W^*W = WW^* = NI,$$

where  $I$  denotes the identity matrix of order  $N$ . The inverse DFT (IDFT) is given by

$$c_j := \frac{1}{N} \sum_{k=0}^{N-1} \widehat{c}_k \omega^{-jk}, \quad j = 0, 1, \dots, N-1,$$

or, in matrix-vector form,

$$\mathbf{c} = \mathcal{F}^{-1}(\widehat{\mathbf{c}}) := W^{-1}\widehat{\mathbf{c}} = \frac{1}{N}W^*\widehat{\mathbf{c}},$$

where  $W^* := \overline{W}^T$  denotes the conjugate transpose of  $W$ .

**Remark 1.** With the above definition of the DFT,  $W$  is the DFT matrix, whereas  $F := W/\sqrt{N}$  is the corresponding unitary Fourier matrix satisfying  $F^*F = FF^* = I$ .

#### 4.2. Circulant matrices

A matrix  $C \in \mathbb{C}^{N \times N}$  is called a circulant matrix if each column vector is obtained from the previous one by a cyclic downward shift. Equivalently, if the first column of  $C$  is  $\mathbf{c} = (c_0, c_1, \dots, c_{N-1})^T$ , then the  $(k, j)$  entry of  $C$  is given by

$$(C)_{k,j} = c_{(k-j) \bmod N}, \quad k, j = 0, 1, \dots, N-1,$$

where the indices are understood modulo  $N$ . In particular,  $c_{-j} = c_{N-j}$  for  $j = 1, 2, \dots, N-1$ . In this case, we write

$$C = \text{circ}(\mathbf{c}), \quad \text{circ}(\mathbf{c}) := \begin{pmatrix} c_0 & c_{N-1} & c_{N-2} & \cdots & c_1 \\ c_1 & c_0 & c_{N-1} & \cdots & c_2 \\ c_2 & c_1 & c_0 & \cdots & c_3 \\ \vdots & \vdots & \vdots & \ddots & \vdots \\ c_{N-1} & c_{N-2} & c_{N-3} & \cdots & c_0 \end{pmatrix}.$$

We consider the eigenvalue problem for the circulant matrix  $C$ :

$$C\mathbf{w}_k = \sigma_k \mathbf{w}_k, \quad \mathbf{w}_k \neq \mathbf{0}, \quad k = 0, 1, \dots, N-1.$$

It is well known that the eigenvalues of  $C$  are given by

$$\sigma_k = \sum_{j=0}^{N-1} c_j \omega^{jk}, \quad k = 0, 1, \dots, N-1, \quad (4.2)$$

which coincides exactly with the DFT of  $\mathbf{c}$ , given in (4.1), and hence  $\sigma_k = \widehat{c}_k$ . For each  $k = 0, 1, \dots, N-1$ , an eigenvector  $\mathbf{w}_k \in \mathbb{C}^N$  of  $C$  corresponding to the eigenvalue  $\sigma_k$  is given by

$$(\mathbf{w}_k)_j := \omega^{-jk}, \quad j = 0, 1, \dots, N-1.$$

Indeed, this can be verified directly as follows. For each  $l = 0, 1, \dots, N-1$ ,

$$\begin{aligned} (C\mathbf{w}_k)_l &= \sum_{j=0}^{N-1} (C)_{l,j} (\mathbf{w}_k)_j = \sum_{j=0}^{N-1} c_{l-j} \omega^{-jk} = \sum_{m=0}^{N-1} c_m \omega^{-(l-m)k} \\ &= \omega^{-lk} \sum_{m=0}^{N-1} c_m \omega^{mk} = \sigma_k \omega^{-lk} = \sigma_k (\mathbf{w}_k)_l, \end{aligned}$$

where the indices are understood modulo  $N$ . Hence, defining the matrix

$$U := (\mathbf{w}_0 \quad \mathbf{w}_1 \quad \cdots \quad \mathbf{w}_{N-1}), \quad (4.3)$$

we obtain the diagonalization

$$U^{-1}CU = \text{diag}(\widehat{\mathbf{c}}),$$

or equivalently,

$$C = U \text{diag}(\widehat{\mathbf{c}})U^{-1},$$

where  $\text{diag}(\widehat{\mathbf{c}})$  denotes the diagonal matrix whose diagonal entries are the components of  $\widehat{\mathbf{c}}$ . Since  $U = W^*$ , where  $W$  is the DFT matrix, this can be rewritten as

$$C = \frac{1}{N} W^* \text{diag}(\widehat{\mathbf{c}})W. \quad (4.4)$$

**Remark 2.** If the DFT and the IDFT are defined by means of the Fourier matrix  $F = W/\sqrt{N}$  as follows:

$$\widehat{\mathbf{c}} = \mathcal{F}(\mathbf{c}) := F\mathbf{c}, \quad \mathbf{c} = \mathcal{F}^{-1}(\widehat{\mathbf{c}}) := F^{-1}\widehat{\mathbf{c}} = F^*\widehat{\mathbf{c}},$$

then the eigenvalues satisfy  $\sigma_k = \sqrt{N} \widehat{c}_k$ , and hence

$$C = F^* \text{diag}(\sqrt{N} \widehat{\mathbf{c}})F.$$

**Remark 3.** Let a circulant matrix  $C$  be defined by

$$(C)_{k,j} = c_{(j-k) \bmod N}, \quad k, j = 0, 1, \dots, N-1,$$

where  $\mathbf{c}^T = (c_0, c_1, \dots, c_{N-1})$  is the first row of  $C$ . Equivalently,  $C$  can be written as

$$C = \begin{pmatrix} c_0 & c_1 & c_2 & \cdots & c_{N-1} \\ c_{N-1} & c_0 & c_1 & \cdots & c_{N-2} \\ c_{N-2} & c_{N-1} & c_0 & \cdots & c_{N-3} \\ \vdots & \vdots & \vdots & \ddots & \vdots \\ c_1 & c_2 & c_3 & \cdots & c_0 \end{pmatrix}.$$

Then, for each  $k = 0, 1, \dots, N-1$ , an eigenvector  $\mathbf{w}_k \in \mathbb{C}^N$  of  $C$  corresponding to the eigenvalue  $\sigma_k$  in (4.2) is given by

$$(\mathbf{w}_k)_j := \omega^{jk}, \quad j = 0, 1, \dots, N-1.$$

If we define  $U$  in the same way as in (4.3), then  $U = W$ . Therefore, the circulant matrix  $C$  is diagonalized as

$$C = \frac{1}{N} W \text{diag}(\widehat{\mathbf{c}}) W^*,$$

Thus, the expression for the diagonalization of a circulant matrix depends on whether the matrix is viewed with respect to its first column or its first row.

#### 4.3. Application to the discrete DtN map

As described in the previous subsection, the matrices  $C_0$  and  $C_1$  appearing in the MFS discretization are circulant because both the source points and collocation points are equally spaced on circles.

Let  $\mathbf{c}_l$  ( $l = 0, 1$ ) denote the first column of  $C_l$ . Applying the diagonalization formula for circulant matrices, we obtain

$$C_l = \frac{1}{N} W^* \text{diag}(\widehat{\mathbf{c}}_l) W, \quad l = 0, 1,$$

where

$$\widehat{\mathbf{c}}_l = \mathcal{F}(\mathbf{c}_l) = W \mathbf{c}_l, \quad \mathbf{c}_l = \mathcal{F}^{-1}(\widehat{\mathbf{c}}_l) = \frac{1}{N} W^* \widehat{\mathbf{c}}_l, \quad l = 0, 1.$$

Hence, the discrete DtN map applied to  $\boldsymbol{\lambda}$  can be written as

$$\begin{aligned} \boldsymbol{\mu} &= \Lambda^{(N)} \boldsymbol{\lambda} = C_1 C_0^{-1} \boldsymbol{\lambda} = \frac{1}{N} W^* \text{diag}(\widehat{\mathbf{c}}_1) \text{diag}(\widehat{\mathbf{c}}_0)^{-1} W \boldsymbol{\lambda} \\ &= \mathcal{F}^{-1}((\mathcal{F}(\mathbf{c}_1) \otimes \mathcal{F}(\mathbf{c}_0) \odot \mathcal{F}(\boldsymbol{\lambda}))), \end{aligned} \quad (4.5)$$

where for two vectors  $\mathbf{a} = (a_0, a_1, \dots, a_{N-1})^T$  and  $\mathbf{b} = (b_0, b_1, \dots, b_{N-1})^T$  in  $\mathbb{C}^N$ , the Hadamard product  $\mathbf{a} \odot \mathbf{b}$  and the Hadamard division  $\mathbf{a} \oslash \mathbf{b}$  are defined, respectively, by

$$\begin{aligned} \mathbf{a} \odot \mathbf{b} &:= (a_0 b_0, a_1 b_1, \dots, a_{N-1} b_{N-1})^T, \\ \mathbf{a} \oslash \mathbf{b} &:= \left( \frac{a_0}{b_0}, \frac{a_1}{b_1}, \dots, \frac{a_{N-1}}{b_{N-1}} \right)^T, \quad b_j \neq 0, \quad j = 0, 1, \dots, N-1. \end{aligned}$$

**Remark 4.** *As noted in Remark 3, the diagonalization formula for a circulant matrix depends on whether the matrix is defined by its first column or by its first row. In the present setting, however, the matrices  $C_l$  ( $l = 0, 1$ ) are symmetric, so this distinction causes no essential difference.*

#### 4.4. FFT-based algorithm

As shown in (4.5), the discrete DtN map can be computed using the DFT and the IDFT, and therefore can be evaluated efficiently by the FFT and the inverse FFT (IFFT). The resulting FFT-based procedure can be summarized as follows.

**Step 1.** Compute the DFTs by the FFT:

$$\widehat{\mathbf{c}}_0 := \mathcal{F}(\mathbf{c}_0), \quad \widehat{\mathbf{c}}_1 := \mathcal{F}(\mathbf{c}_1), \quad \widehat{\boldsymbol{\lambda}} := \mathcal{F}(\boldsymbol{\lambda}).$$

**Step 2.** Compute

$$\widehat{\mathbf{r}} := \widehat{\mathbf{c}}_1 \circledast \widehat{\mathbf{c}}_0,$$

which coincides with the DFT of the first column of  $\Lambda^{(N)}$ . Therefore, the discrete DtN map can be efficiently computed as

$$\Lambda^{(N)} = \text{circ}(\mathcal{F}^{-1}(\widehat{\mathbf{r}})).$$

**Step 3.** Compute

$$\widehat{\boldsymbol{\mu}} := \widehat{\mathbf{r}} \odot \widehat{\boldsymbol{\lambda}}.$$

**Step 4.** Compute the IDFT by the IFFT:

$$\boldsymbol{\mu} := \mathcal{F}^{-1}(\widehat{\boldsymbol{\mu}}).$$

A straightforward computation of  $C_1 C_0^{-1} \boldsymbol{\lambda}$  ( $= \boldsymbol{\mu}$ ) requires first solving the dense linear system (3.2), corresponding to (3.3), at a cost of  $O(N^3)$  operations, and then evaluating (3.4), which requires a further  $O(N^2)$  operations. Thus, the direct approach involves dense-matrix computations.

By contrast, the present method exploits the circulant structure of  $C_0$  and  $C_1$ . As described above, the FFT enables the overall computation to be carried out in  $O(N \log N)$  operations, without explicitly solving a dense system of linear equations. Moreover, since each of the circulant matrices  $C_0$  and  $C_1$  is completely determined by its first column, it suffices to store only these columns. As a result, the memory requirement is reduced from  $O(N^2)$  to  $O(N)$ . Hence, the proposed approach significantly reduces both the computational and memory costs.

In particular, since (3.3) can be written as

$$\boldsymbol{\alpha} = C_0^{-1} \boldsymbol{\lambda} = \frac{1}{N} W^* \text{diag}(\widehat{\mathbf{c}}_0)^{-1} W \boldsymbol{\lambda} = \mathcal{F}^{-1}(\mathcal{F}(\boldsymbol{\lambda}) \circledast \mathcal{F}(\mathbf{c}_0)),$$

the unknown expansion coefficients can be computed efficiently by the FFT, without directly solving the linear system (3.2).

## 5. Finite element formulation with the transparent boundary condition

In this section, we briefly explain how the transparent boundary condition (TBC) is incorporated into the finite element method (FEM) for the interior problem posed in  $\Omega$ .

Multiplying the Helmholtz equation (2.5a) by a test function  $v$ , which should not be confused with the exterior solution introduced earlier, and applying Green's formula, we obtain

$$\int_{\Omega} \nabla u \cdot \nabla v \, d\Omega - \kappa^2 \int_{\Omega} uv \, d\Omega - \int_{\Gamma_0} (\Lambda u) v \, d\Gamma = \int_{\Omega} f v \, d\Omega$$

for all test functions  $v \in H^1(\Omega)$  satisfying  $v = 0$  on  $\Gamma$ .

Let  $V_h \subset H^1(\Omega)$  be the finite element space consisting of piecewise linear functions. Let  $g_h$  and  $f_h$  denote the discrete approximations of  $g$  and  $f$ , respectively. We seek  $u_h \in V_h$  such that

$$u_h = g_h \quad \text{on} \quad \Gamma,$$

and

$$\int_{\Omega} \nabla u_h \cdot \nabla v_h \, d\Omega - \kappa^2 \int_{\Omega} u_h v_h \, d\Omega - \int_{\Gamma_0} (\Lambda^{(N)} u_h) v_h \, d\Gamma = \int_{\Omega} f_h v_h \, d\Omega$$

for all  $v_h \in V_h$  satisfying  $v_h = 0$  on  $\Gamma$ , where  $\Lambda^{(N)}$  denotes the discrete DtN map on  $\Gamma_0$ .

Let  $\{\phi_j\}_{j=1}^M$  be the nodal basis functions of  $V_h$ . Then the finite element solution  $u_h \in V_h$  is expressed as

$$u_h = \sum_{j=1}^M u_j \phi_j,$$

where  $\mathbf{u} = (u_1, \dots, u_M)^\top$  denotes the coefficient vector.

We order the nodal degrees of freedom according to the nodes in  $\Omega$ , on  $\Gamma$ , and on  $\Gamma_0$ . Accordingly, the coefficient vector is decomposed as

$$\mathbf{u} = \begin{pmatrix} \mathbf{u}_{\Omega} \\ \mathbf{u}_{\Gamma} \\ \mathbf{u}_{\Gamma_0} \end{pmatrix}.$$

With this ordering, we introduce the block matrix

$$A = \begin{pmatrix} A_{\Omega\Omega} & A_{\Omega\Gamma} & A_{\Omega\Gamma_0} \\ A_{\Gamma\Omega} & A_{\Gamma\Gamma} & A_{\Gamma\Gamma_0} \\ A_{\Gamma_0\Omega} & A_{\Gamma_0\Gamma} & A_{\Gamma_0\Gamma_0} \end{pmatrix},$$

whose blocks are defined by

$$(A_{XY})_{k,j} = \int_{\Omega} \nabla \phi_j^{(Y)} \cdot \nabla \phi_k^{(X)} \, d\Omega - \kappa^2 \int_{\Omega} \phi_j^{(Y)} \phi_k^{(X)} \, d\Omega, \quad X, Y \in \{\Omega, \Gamma, \Gamma_0\}$$

with  $\phi_j^{(Y)}$  and  $\phi_k^{(X)}$  denoting the basis functions associated with the nodes belonging to  $Y$  and  $X$ , respectively.

Similarly, the load vector is decomposed as

$$\mathbf{f} = \begin{pmatrix} \mathbf{f}_\Omega \\ \mathbf{f}_\Gamma \\ \mathbf{f}_{\Gamma_0} \end{pmatrix}$$

with

$$(\mathbf{f}_X)_k = \int_\Omega f_h \phi_k^{(X)} d\Omega, \quad X \in \{\Omega, \Gamma, \Gamma_0\}.$$

Since the DtN map acts only on  $\Gamma_0$ , its contribution appears only in the  $(\Gamma_0, \Gamma_0)$  block. Then the full system is written as

$$\begin{pmatrix} A_{\Omega\Omega} & A_{\Omega\Gamma} & A_{\Omega\Gamma_0} \\ A_{\Gamma\Omega} & A_{\Gamma\Gamma} & A_{\Gamma\Gamma_0} \\ A_{\Gamma_0\Omega} & A_{\Gamma_0\Gamma} & A_{\Gamma_0\Gamma_0} - \Lambda^{(N)} \end{pmatrix} \begin{pmatrix} \mathbf{u}_\Omega \\ \mathbf{u}_\Gamma \\ \mathbf{u}_{\Gamma_0} \end{pmatrix} = \begin{pmatrix} \mathbf{f}_\Omega \\ \mathbf{f}_\Gamma \\ \mathbf{f}_{\Gamma_0} \end{pmatrix}.$$

Since the Dirichlet boundary condition is prescribed on  $\Gamma$ , we have

$$\mathbf{u}_\Gamma = \mathbf{g},$$

where  $\mathbf{g}$  denotes the vector of nodal values of the prescribed boundary data on  $\Gamma$ . Therefore, the unknowns are reduced to  $\mathbf{u}_\Omega$  and  $\mathbf{u}_{\Gamma_0}$ , and the resulting reduced system becomes

$$\begin{pmatrix} A_{\Omega\Omega} & A_{\Omega\Gamma_0} \\ A_{\Gamma_0\Omega} & A_{\Gamma_0\Gamma_0} - \Lambda^{(N)} \end{pmatrix} \begin{pmatrix} \mathbf{u}_\Omega \\ \mathbf{u}_{\Gamma_0} \end{pmatrix} = \begin{pmatrix} \mathbf{f}_\Omega \\ \mathbf{f}_{\Gamma_0} \end{pmatrix} - \begin{pmatrix} A_{\Omega\Gamma} \\ A_{\Gamma_0\Gamma} \end{pmatrix} \mathbf{g}.$$

This is the final linear system to be solved.

## 6. Numerical examples

### 6.1. Accuracy of the discrete DtN map

We verify the accuracy of the discrete DtN map constructed by the MFS through comparison with an exact solution [16].

The radius of the circular artificial boundary  $\Gamma_0$  is taken as  $R_0 = 1$ , and the wavenumber is set to  $\kappa = 30$ . The exact solution is given by

$$v(re^{i\theta}) := \frac{H_1^{(1)}(\kappa r)}{H_1^{(1)}(\kappa)} \cos \theta, \quad r > 1, \quad 0 \leq \theta < 2\pi.$$

Figure 2 shows the real part of the exact solution in the subdomain  $D := (-3, 3)^2$ , which is identified with the rectangular domain

$$\{z = x + iy \in \mathbb{C} : -3 < x < 3, -3 < y < 3\}.$$

In this case, the normal derivative of  $v$  on  $\Gamma_0$  is obtained as

$$\frac{\partial v}{\partial n}(e^{i\theta}) = -\frac{\kappa}{2H_1^{(1)}(\kappa)} \left( H_0^{(1)}(\kappa) - H_2^{(1)}(\kappa) \right) \cos \theta, \quad 0 \leq \theta < 2\pi.$$

Taking the exact solution  $v$  as the unknown function, we solve Problem (2.4) with the Dirichlet data  $\lambda(\theta) := \cos \theta$ .

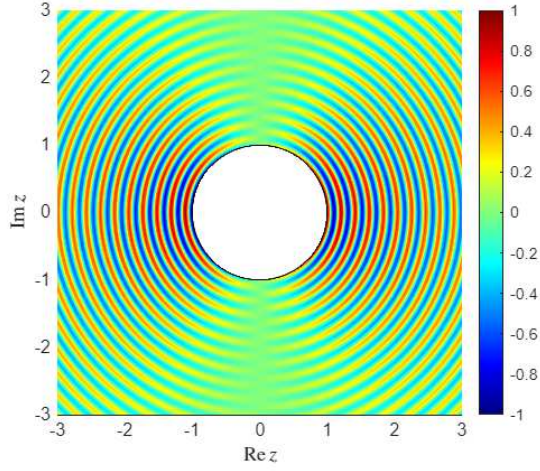


Figure 2: Exact solution in  $D$

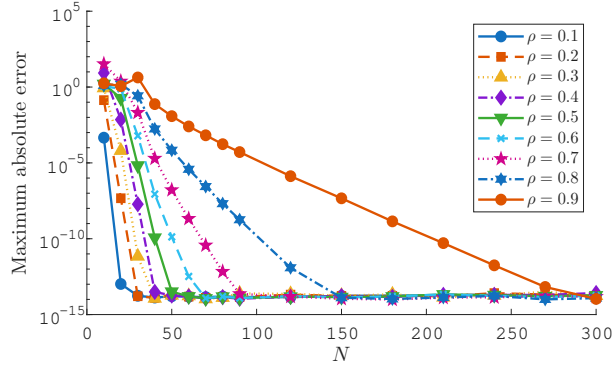


Figure 3: Maximum absolute error versus  $N$  for various values of  $\rho$

Figure 3 shows a semi-logarithmic plot in which the horizontal axis represents the number of collocation points  $N$  and the vertical axis represents the maximum absolute error in the subdomain  $D$ . The number of collocation points was chosen

in the range  $10 \leq N \leq 90$  with increments of 10, and  $90 \leq N \leq 300$  with increments of 30.

Each curve corresponds to a different value of  $\rho$ , and the results for  $\rho = 0.1$  to  $\rho = 0.9$  are shown in the legend. The error decreases overall as  $N$  increases. When  $\rho$  is small, the error decays rapidly as  $N$  increases and reaches machine precision. As  $\rho$  becomes larger, however, the convergence becomes significantly slower. Nevertheless, before reaching machine precision, the error still shows an approximately exponential decay. These results indicate that, also for the Helmholtz equation, the error decays exponentially with respect to  $N$ , as observed for the MFS applied to the Laplace equation [8].

Next, for the parameters  $N = 300$  and  $\rho = 0.9$ , Fig. 4 shows the common logarithm of the absolute error of the real part of the numerical solution,

$$\log_{10} |\operatorname{Re} v(z) - \operatorname{Re} v^{(N)}(z)|, \quad z \in D.$$

It can be observed that the absolute error is less than approximately  $10^{-14}$ , indicating that a highly accurate numerical solution is obtained.

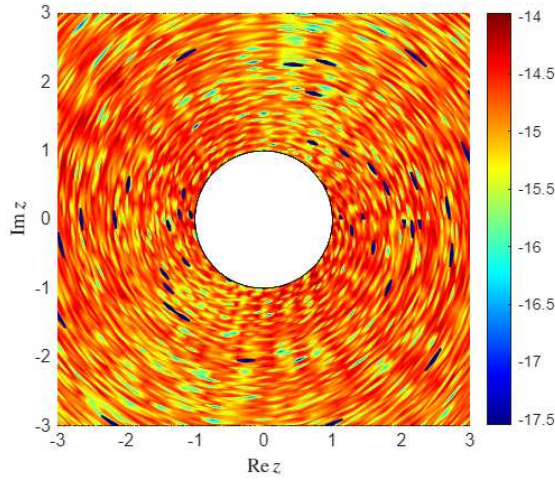


Figure 4: Absolute errors in  $D$  ( $\log_{10}$  scale)

Furthermore, on  $\Gamma_0$  ( $r = 1$ ,  $0 \leq \theta < 2\pi$ ), the absolute error of the real part of the numerical solution

$$|\operatorname{Re} v(e^{i\theta}) - \operatorname{Re} v^{(N)}(e^{i\theta})|, \quad 0 \leq \theta < 2\pi$$

and the absolute error of the real part of the normal derivative

$$\left| \operatorname{Re} \frac{\partial v(e^{i\theta})}{\partial n} - \operatorname{Re} \frac{\partial v^{(N)}(e^{i\theta})}{\partial n} \right|, \quad 0 \leq \theta < 2\pi$$

are shown as B.V. and N.D. in Fig. 5, respectively. This result indicates that the discrete DtN map functions properly and that the normal derivative on the boundary is computed with sufficient accuracy.

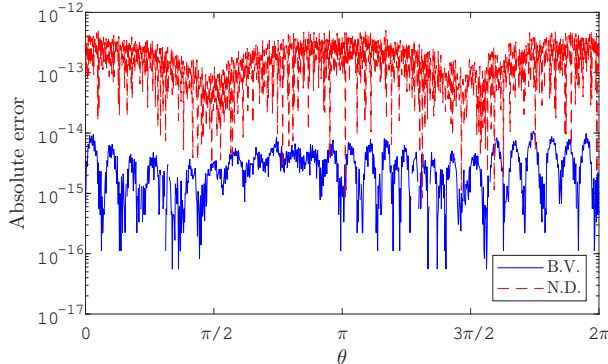


Figure 5: Absolute errors in the real part of  $v^{(N)}$  and its normal derivative on  $\Gamma_0$

## 6.2. Computational efficiency of the discrete DtN map

We next examine the computational efficiency of the discrete DtN map. All computation times reported in this section were measured in MATLAB R2025b on the same computing environment for both methods. The experiments were performed on a PC equipped with an AMD Ryzen 5 7430U processor and 16 GB of memory. For each value of  $N$ , the reported computation time is the average of three runs.

Figure 6 shows the computation time for constructing the discrete DtN map as a function of  $N$ . The results clearly show that the proposed method is significantly faster than the direct method. As  $N$  increases, the computation time of the direct method grows rapidly, whereas that of the proposed method increases much more mildly. Moreover, the observed growth is consistent with the expected complexities  $O(N^3)$  for the direct method and  $O(N \log N)$  for the proposed FFT-based method. This behavior reflects the fact that the direct method requires the solution of a dense linear system, while the proposed method exploits the circulant structure of the discretized operators and evaluates the discrete DtN map efficiently by the FFT. It is also worth noting that, even for relatively large values of  $N$ , the proposed method remains faster than the direct method for much smaller values of  $N$ . This clearly demonstrates the practical effectiveness of the FFT-based acceleration.

To further illustrate the gain in efficiency, Figure 7 plots the ratio of the computation time of the direct method to that of the proposed method. The ratio increases as  $N$  becomes larger, showing that the advantage of the proposed method becomes more pronounced for finer discretizations. In particular, for large values of  $N$ , the FFT-based method achieves a substantial reduction in computational cost compared with the direct method. These results confirm that the proposed approach achieves substantial computational savings.

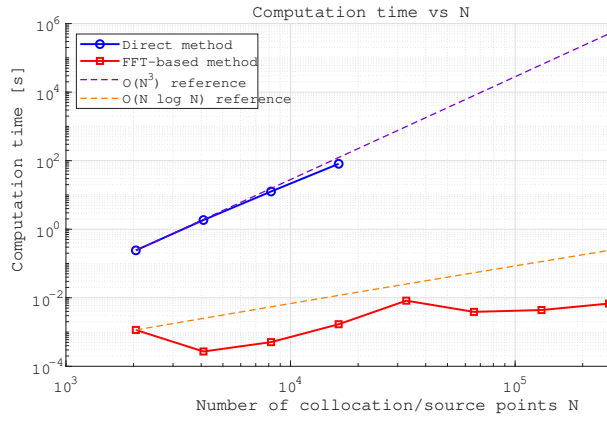


Figure 6: Computation time for constructing the discrete DtN map versus the number of collocation points  $N$

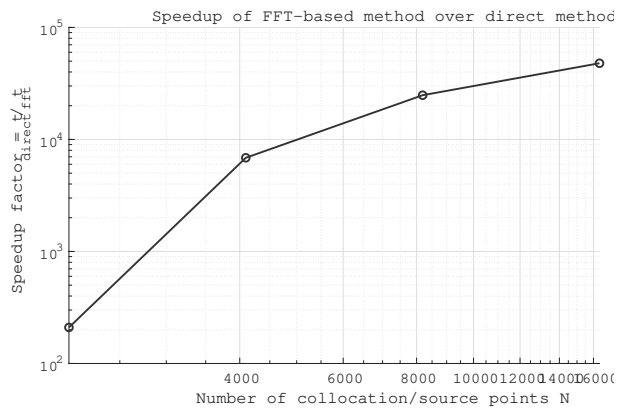


Figure 7: Ratio of the computation time of the direct method to that of the proposed FFT-based method

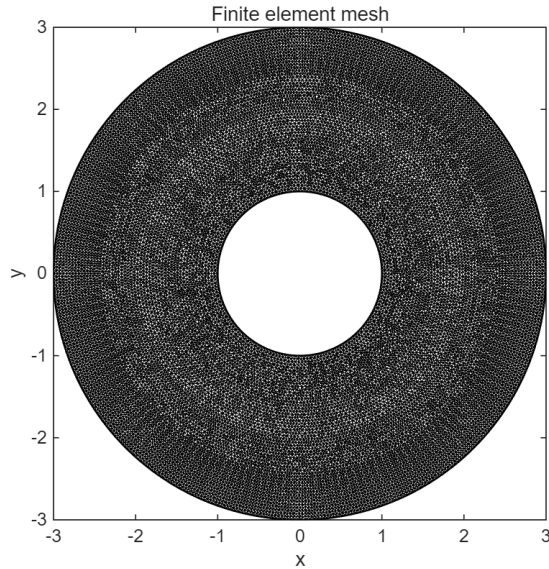


Figure 8: Finite element mesh (19,320 nodes and 37,974 elements)

### 6.3. Numerical verification of the TBC

In this example, we verify that, by incorporating the DtN-based TBC into the FEM formulation, the original exterior problem on an unbounded domain can be successfully solved on a bounded computational domain.

We consider the homogeneous case  $f = 0$  with a circular boundary  $\Gamma$  of radius  $R(\theta) := 1$ . As an exact solution, we use the single outgoing Fourier–Hankel mode

$$u(re^{i\theta}) = \frac{H_m^{(1)}(\kappa r)}{H_m^{(1)}(\kappa R_0)} e^{im\theta}, \quad r > 1, \quad 0 \leq \theta < 2\pi,$$

which satisfies the Helmholtz equation in the exterior domain and the radiation condition. The Dirichlet boundary data on  $\Gamma$  are taken from this exact solution. We choose the mode number  $m = 3$ .

In the computation, we set  $\kappa = 8$ ,  $R_0 = 3$ ,  $N = 500$ , and  $\rho = 0.99R_0$ . Figure 8 shows the finite element mesh used in the computation for the linear finite element approximation. The resulting mesh consists of 19,320 nodes and 37,974 elements, and the maximum mesh size is  $h = 0.0660$ . Figure 9 displays the real part  $\text{Re } u$  of the exact solution, while Figure 10 shows the corresponding finite element solution  $\text{Re } u_h$  obtained with the proposed TBC. The two plots are visually almost indistinguishable, indicating that the finite element solution successfully reproduces the main profile and oscillatory behavior of the exact solution. This observation is supported by Figure 11, which shows that the

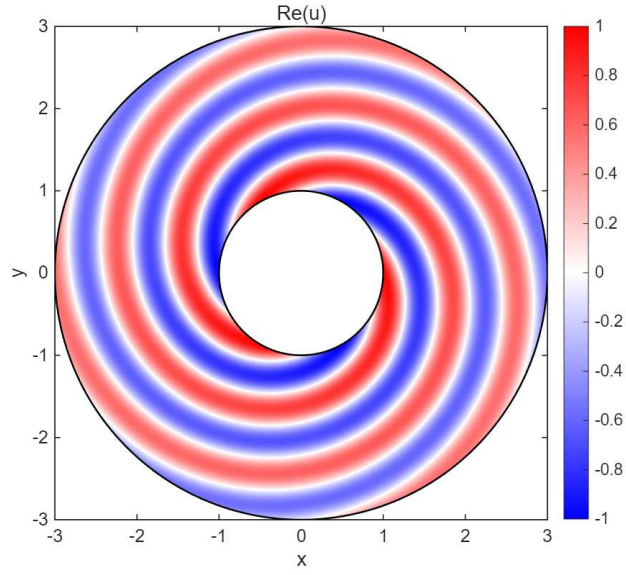


Figure 9: Real part of the exact solution

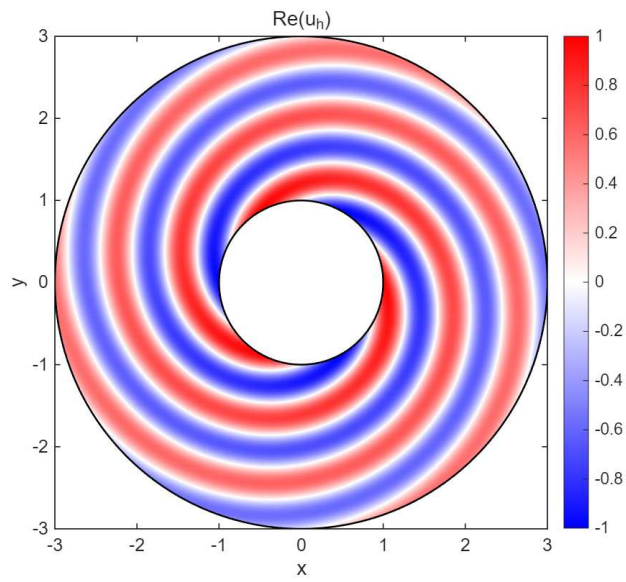


Figure 10: Real part of the finite element solution

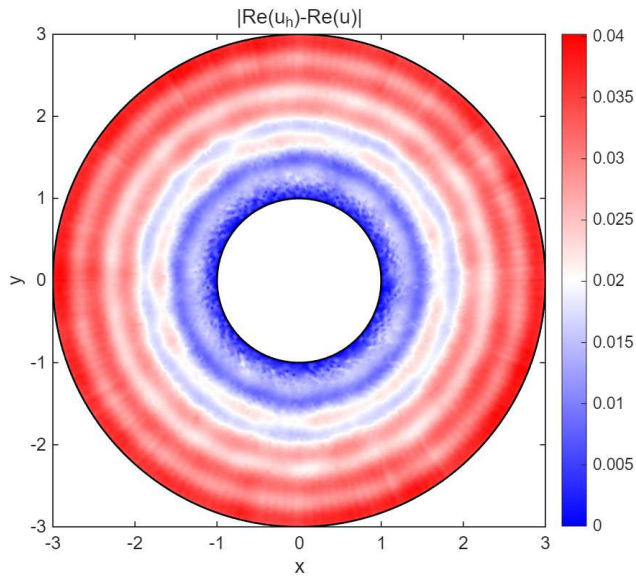


Figure 11: Numerical error

error remains small over the whole computational domain, except for slight local increases near the artificial boundary; in particular, the maximum error is

$$\|u_h - u\|_{C(\bar{\Omega})} = 0.0402.$$

No noticeable deterioration appears near the artificial boundary, which indicates that the proposed TBC introduces no artificial reflections and accurately represents the exterior behavior. These results confirm that the proposed TBC is correctly incorporated into the finite element formulation and provides an accurate and reliable boundary treatment for the exterior Helmholtz problem.

#### 6.4. Inhomogeneous problem with an irregular boundary

This example is designed to verify that the proposed FEM–DtN coupling remains accurate for an exterior Helmholtz problem with an irregular boundary and a compactly supported inhomogeneous term. The boundary  $\Gamma$  is given by

$$R(\theta) = 0.55 + 0.10 \cos(3\theta) + 0.06 \sin(5\theta) + 0.04 \cos(7\theta + 0.3), \quad 0 \leq \theta < 2\pi.$$

To validate the proposed method, we use a manufactured exact solution consisting of a compactly supported part and an outgoing radiating part,

$$u = u_c + u_r,$$

so that the corresponding inhomogeneous term

$$f := -(\Delta u + \kappa^2 u)$$

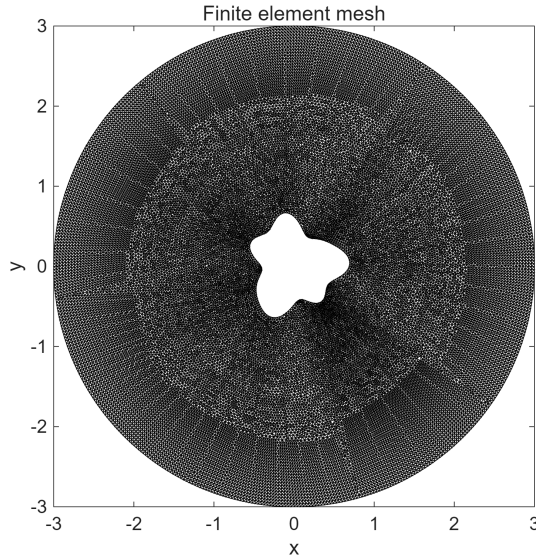


Figure 12: Finite element mesh (28,494 nodes and 56,322 elements)

is compactly supported in  $\Omega$ . The detailed construction of  $u$  and  $f$  is given in Appendix A.

In the computation, we set  $\kappa = 8$ ,  $R_0 = 3$ ,  $N = 500$ , and  $\rho = 0.99R_0$ . The resulting boundary value problem is discretized in  $\Omega$  by the FEM using piecewise linear triangular elements. Figure 12 shows the finite element mesh used in the computation. The resulting mesh consists of 28,494 nodes and 56,322 elements, and the maximum mesh size is  $h = 0.0671$ .

The real part of the inhomogeneous term, the exact solution, the numerical solution, and the absolute error are shown in Figures 13–16, respectively. The numerical solution is in good agreement with the exact solution, indicating that the finite element approximation successfully captures the main features of the solution. This observation is also supported by Figure 16, where the absolute error is seen to remain small throughout the computational domain, except for slight local increases near the artificial boundary and in regions where the solution varies rapidly.

Finally, the numerical solution  $u_h$  is compared with  $u$  through the maximum error

$$\|u_h - u\|_{C(\bar{\Omega})} = 0.0295.$$

This result confirms the effectiveness of the proposed method for exterior inhomogeneous Helmholtz problems with an irregular boundary.

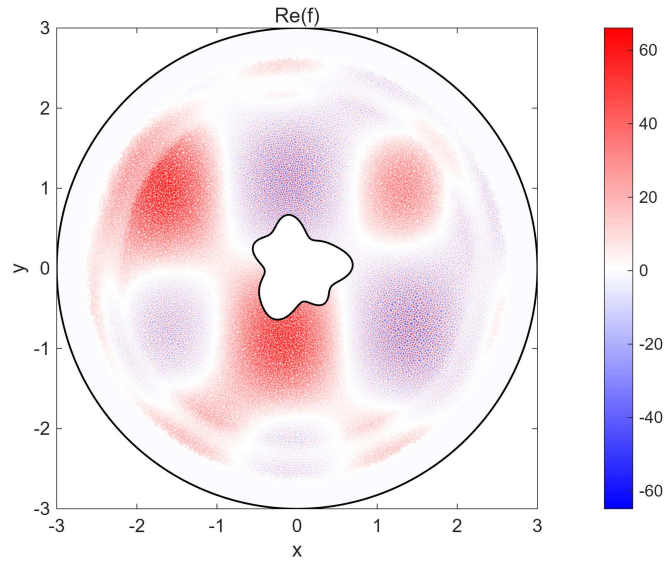


Figure 13: Real part of inhomogeneous term

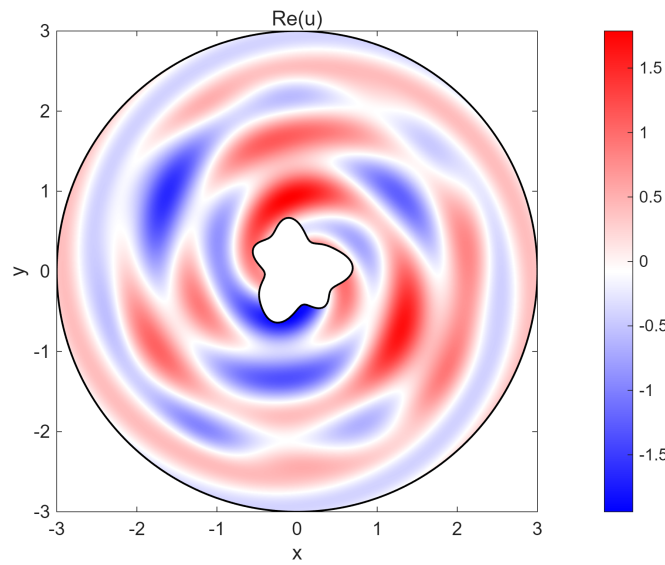


Figure 14: Exact solution

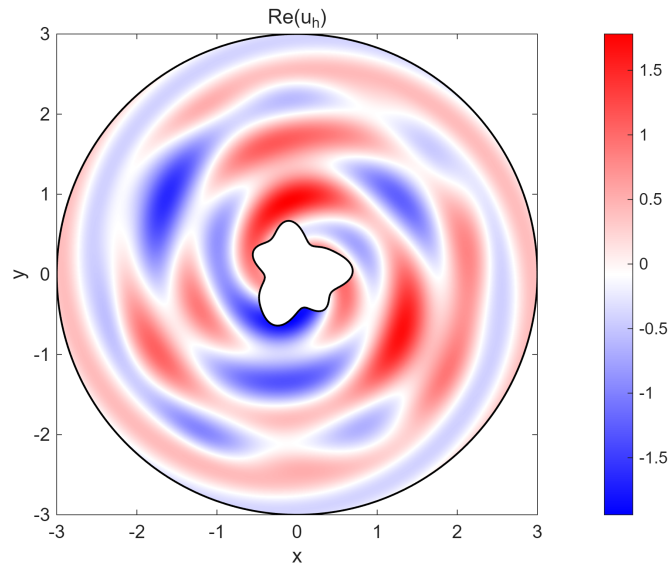


Figure 15: Finite element solution

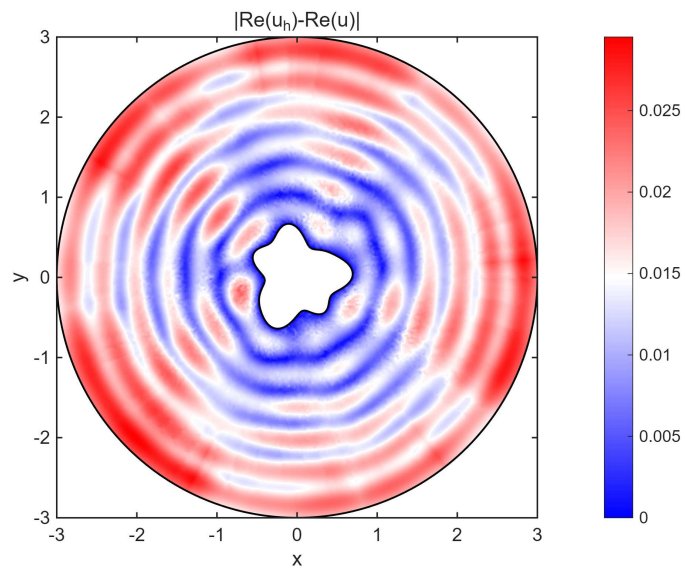


Figure 16: Numerical error

## 7. Conclusions

In this paper, we proposed a numerical method for directly solving the exterior Dirichlet problem for the two-dimensional inhomogeneous Helmholtz equation in an unbounded domain, based on a domain decomposition approach combined with a numerically constructed DtN map.

The DtN map is discretized by the MFS, leading to a circulant matrix representation. Hence, it can be applied efficiently by the FFT, even when the number of collocation points is large. The numerical examples play distinct roles. The first example focuses on the performance of the proposed method for large wavenumbers, while the second and third examples are included to confirm the validity of the FEM incorporating the DtN-based TBC.

By incorporating the TBC defined through the DtN map into the finite element discretization, the original problem in the unbounded domain is reduced to a problem posed on a bounded computational domain. In this way, the proposed approach enables the FEM to handle exterior problems that cannot be treated directly by a standard finite element formulation on a bounded domain alone. Furthermore, since the present framework also applies to inhomogeneous equations, it overcomes a difficulty of the classical boundary element method, which becomes less straightforward in the presence of inhomogeneous terms.

From a theoretical viewpoint, it is known that the DtN map defined on a circular boundary is diagonal with respect to the Fourier basis [2], that is, the Fourier basis forms an eigenfunction system of the DtN map. This property corresponds to the fact that the circulant matrix representing the discrete DtN map obtained by the MFS is diagonalized by the DFT matrix. From this perspective, it is also of interest to investigate in what topology the matrix representing the discrete DtN map converges to the true DtN map as the number of collocation points tends to infinity.

Furthermore, when three-dimensional problems are considered, the discrete DtN map does not become a simple circulant matrix. However, it becomes a block matrix whose components are circulant matrices [10]. Therefore, the idea of the proposed method can be extended to three-dimensional problems.

### Appendix A. Construction of the manufactured solution for the inhomogeneous problem

We describe the construction of a manufactured solution used in Section 6.4 for the inhomogeneous exterior Helmholtz problem with an irregular boundary.

Although the main text identifies  $\mathbb{R}^2$  with  $\mathbb{C}$ , in this appendix we describe the manufactured solution in Cartesian coordinates  $(x, y) \in \mathbb{R}^2$  for clarity.

We write the solution in the form

$$u = u_c + u_r,$$

where  $u_c$  is introduced to generate a compactly supported inhomogeneous term, whereas  $u_r$  is an outgoing homogeneous solution ensuring that the solution does not vanish outside the artificial boundary.

*Compactly supported part*

The first part is defined by

$$u_c(x, y) := \chi(r) p(x, y), \quad r := \sqrt{x^2 + y^2},$$

where  $p$  is the smooth real-valued function

$$p(x, y) := \cos(2.1x + 0.3) \sin(1.7y - 0.2) + 0.15x + 0.10y.$$

The cutoff function  $\chi$  is chosen so that it is equal to 1 near the boundary  $\Gamma$  and vanishes near the artificial boundary  $\Gamma_0$ . More precisely, for two radii  $0 < R_1 < R_2 < R_0$ , we define

$$\chi(r) := \begin{cases} 1, & 0 \leq r \leq R_1, \\ 1 - S\left(\frac{r - R_1}{R_2 - R_1}\right), & R_1 < r < R_2, \\ 0, & r \geq R_2, \end{cases}$$

where

$$S(s) := 10s^3 - 15s^4 + 6s^5.$$

In the computation, we take

$$R_1 = 0.72R_0, \quad R_2 = 0.88R_0.$$

Since  $\chi(r) = 0$  for  $r \geq R_2$ , the function  $u_c$  vanishes in a neighborhood of the artificial boundary  $\Gamma_0$ .

*Outgoing radiating part*

The second part is chosen as a single outgoing Fourier–Hankel mode,

$$u_r(r \cos \theta, r \sin \theta) := \beta \frac{H_m^{(1)}(\kappa r)}{H_m^{(1)}(\kappa R_0)} e^{im\theta}.$$

where, as stated in the main text,  $H_m^{(1)}$  denotes the Hankel function of the first kind. In the present example, the parameters are chosen as

$$m = 2, \quad \beta = 0.35 + 0.20i.$$

By construction,  $u_r$  satisfies

$$\Delta u_r + \kappa^2 u_r = 0$$

in the computational domain and represents an outgoing wave outside the artificial boundary. Therefore, although the inhomogeneous term is compactly supported, the solution itself does not vanish outside  $\Gamma_0$ .

*Inhomogeneous term*

The inhomogeneous term is defined by

$$f := -(\Delta u + \kappa^2 u).$$

Since  $u_r$  satisfies the homogeneous Helmholtz equation, we obtain

$$f = -(\Delta u_c + \kappa^2 u_c).$$

Substituting  $u_c = \chi p$ , we have

$$f = -(\Delta(\chi p) + \kappa^2 \chi p) = -(p \Delta \chi + 2 \nabla \chi \cdot \nabla p + \chi \Delta p + \kappa^2 \chi p).$$

The derivatives of  $p$  are given by

$$\nabla p = \begin{pmatrix} -2.1 \sin(2.1x + 0.3) \sin(1.7y - 0.2) + 0.15 \\ 1.7 \cos(2.1x + 0.3) \cos(1.7y - 0.2) + 0.10 \end{pmatrix},$$

and

$$\Delta p = -(2.1^2 + 1.7^2) \cos(2.1x + 0.3) \sin(1.7y - 0.2).$$

Since  $\chi$  depends only on  $r = \sqrt{x^2 + y^2}$ , we also have

$$\nabla \chi(r) = \chi'(r) \frac{1}{r} \begin{pmatrix} x \\ y \end{pmatrix}, \quad \Delta \chi(r) = \chi''(r) + \frac{1}{r} \chi'(r), \quad r > 0.$$

Hence, the support of  $f$  is contained in the annular domain

$$\text{supp } f \subset \{(x, y) \in \mathbb{R}^2 : R_1 \leq \sqrt{x^2 + y^2} \leq R_2\},$$

so that  $f$  is compactly supported in the computational domain.

*Boundary data*

The Dirichlet boundary data on  $\Gamma$  are taken from the solution,

$$g = u|_{\Gamma}.$$

On the artificial boundary  $\Gamma_0$ , the TBC is imposed. Since  $u_c$  vanishes near  $\Gamma_0$ , both  $u$  and  $\partial u / \partial n$  on  $\Gamma_0$  are determined solely by  $u_r$ .

## References

- [1] Barnett, A. H. and Betcke, T.: Stability and convergence of the method of fundamental solutions for Helmholtz problems on analytic domains, *Journal of Computational Physics*, **227**, (2008), 7003–7026.
- [2] Binford, T. L. *et al.*: Exact non-reflecting boundary conditions on perturbed domains and hp-finite elements, *Journal of Scientific Computing*, **39** (2009), 265–292.

- [3] Bogomolny, A.: Fundamental solutions method for elliptic boundary value problems, *SIAM Journal on Numerical Analysis*, **22**, 4 (1985), 644–669.
- [4] Davis, P. J.: Circulant Matrices, Second edition, AMS Chelsea Publishing (2012).
- [5] Du, Q. and Yu, D.: Dirichlet–Neumann alternating algorithm based on the natural boundary reduction for time-dependent problems over an unbounded domain, *Applied Numerical Mathematics*, **44** (2003), 471–486.
- [6] Ei, S. *et al.*: Method of fundamental solutions for Neumann problems of the modified Helmholtz equation in disk domains, *Journal of Computational and Applied Mathematics*, **402**, (2022), 113795.
- [7] Katsurada, M. and Okamoto, H.: A mathematical study of the charge simulation method I, *Journal of the Faculty of Science, the University of Tokyo, Section 1A Mathematics*, **35** (1988), 507–518.
- [8] Katsurada, M.: A mathematical study of the charge simulation method II, *Journal of the Faculty of Science, the University of Tokyo, Section 1A Mathematics*, **36** (1989), 135–162.
- [9] Liu, B. and Du, Q.: Dirichlet–Neumann alternating algorithm for an Exterior anisotropic quasilinear elliptic problem, *Applications of Mathematics*, **59** (2014), 285–301.
- [10] Liu, X.-Y. *et al.*: A Kansa-radial basis function method for elliptic boundary value problems in annular domains, *Journal of Scientific Computing*, **65** (2015), 1240–1269.
- [11] Liu, X.-Y. *et al.*: Conformal mapping for the efficient solution of Poisson problems with the Kansa-RBF method, *Journal of Scientific Computing*, **71** (2017), 1035–1061.
- [12] Lu, T. *et al.*: Domain Decomposition Method — New Techniques for Numerical Methods of Partial Differential Equations, Science Press (1999) (*in Chinese*).
- [13] Mathon, R. and Johnston, R. L.: The approximate solution of elliptic boundary-value problems by fundamental solutions, *SIAM Journal on Numerical Analysis*, **14**, 4 (1977), 638–650.
- [14] Nicholls, D. P. and Nigam, N.: Exact non-reflecting boundary conditions on general domains, *Journal of Computational Physics*, **194** (2004), 278–303.
- [15] Shigeta, T.: Mathematically improved convergence analysis for the non-overlapping domain decomposition method, *Engineering Analysis with Boundary Elements*, **166** (2024), 105805.

- [16] Shigeta, T.: Efficient numerical computation of the Dirichlet-to-Neumann map for an exterior Dirichlet problem of the two-dimensional Helmholtz equation, *Transactions of the Japan Society for Computational Methods in Engineering*, **25** (2025), 71–75 (*in Japanese*).
- [17] Smyrlis, Y.-S. and Karageorghis, A.: Efficient implementation of the MFS: The three scenarios, *Journal of Computational and Applied Mathematics*, **227** (2009), 83–92.
- [18] Yu, D. *et al.*: A Dirichlet–Neumann alternating method in infinite domain: Algorithm and convergence analysis, *Research Report ICM–95–31*, Institute of Computational Mathematics and Scientific/Engineering Computing, Chinese Academy of Sciences (1995).
- [19] Yu, D.: Discretization of non-overlapping domain decomposition method for unbounded domains and its convergence, *Chinese Journal of Numerical Mathematics and Applications*, **18**, 4 (1996), 93–102.